Geophys. J. Int. (1997) **130**, 422–434

Recovering magnetic susceptibility from electromagnetic data over a one-dimensional earth

Zhiyi Zhang and Douglas W. Oldenburg

UBC-Geophysical Inversion Facility, Department of Earth and Ocean Sciences, University of British Columbia, Vancouver, BC, Canada, V6T 1Z4.
E-mail: oldenburg@geop.ubc.ca

Accepted 1997 April 7. Received 1996 December 4; in original form 1996 April 18

SUMMARY

While the inversion of electromagnetic data to recover electrical conductivity has received much attention, the inversion of those data to recover magnetic susceptibility has not been fully studied. In this paper we invert frequency-domain electromagnetic (EM) data from a horizontal coplanar system to recover a 1-D distribution of magnetic susceptibility under the assumption that the electrical conductivity is known. The inversion is carried out by dividing the earth into layers of constant susceptibility and minimizing an objective function of the susceptibility subject to fitting the data. An adjoint Green's function solution is used in the calculation of sensitivities, and it is apparent that the sensitivity problem is driven by three sources. One of the sources is the scaled electric field in the layer of interest, and the other two, related to effective magnetic charges, are located at the upper and lower boundaries of the layer. These charges give rise to a frequency-independent term in the sensitivities. Because different frequencies penetrate to different depths in the earth, the EM data contain inherent information about the depth distribution of susceptibility. This contrasts with static field measurements, which can be reproduced by a surface layer of magnetization. We illustrate the effectiveness of the inversion algorithm on synthetic and field data and show also the importance of knowing the background conductivity. In practical circumstances, where there is no *a priori* information about conductivity distribution, a simultaneous inversion of EM data to recover both electrical conductivity and susceptibility will be required.

Key words: electromagnetic data, electromagnetic survey, horizontal loop, inversion, magnetic susceptibility.

INTRODUCTION

Electromagnetic data are sensitive to conductivity σ, magnetic permeability μ and electrical permittivity ε. The decay of the EM fields in the Earth depends upon these parameters and the frequency of the source. It follows that a multifrequency sounding contains information about all of these properties as a function of depth and, in principle, it is possible to invert simultaneously any set of data for σ, μ and ε. The first step in this process of simultaneous inversion is to be able to invert for any one of the parameters when the others are specified. Electrical conductivity characteristically varies by orders of magnitude and there have been numerous papers devoted to recovering σ when μ and ε have been specified. Relative electrical permittivity varies from about 1 to 80 (Keller 1990), and this parameter has received much attention for surveys carried out at high frequency. Although relative magnetic permeability may vary from 1 to 20 for various rocks and minerals, in practice it varies from 1 to less than 2.0. The effect of such small variations can often be ignored and EM data are commonly inverted after employing the assumption that $\mu = \mu_0$, the relative permeability of free space. Nevertheless, there are instances where permeability changes alter the data in a significant way. A well-known example of this is the negative in-phase data measured with a typical frequency-domain airborne electromagnetic (AEM) system. Those negative data cannot be the response of a purely conductive model. Magnetic permeability greater than μ_0, or equivalently positive magnetic susceptibility, must exist.

Magnetic susceptibility is an important physical parameter in geophysical surveys, but the usual way to obtain information about the distribution of susceptibility is through the inversion of static magnetic data obtained from usual magnetic surveys. Unfortunately these data can be reproduced by a layer of susceptible material at the Earth's surface. This illustrates not only the extreme non-uniqueness inherent in the interpretation of magnetic data but also that there is no inherent information about the susceptibility distribution with depth. Algorithms which obtain depth distributions do so by imposing parametrization on the model domain (Bhattacharyya 1980; Zeyen & Pous 1991; Wang & Hansen 1990), by applying constraints to the solution (Last & Kubik 1983; Guillen & Menichetti 1984) or by introducing a depth weighting function to counteract the natural decay of the kernel functions. An example of this last approach is given in Li & Oldenburg (1996).

Rigorous inversion of EM data to estimate the distribution of magnetic susceptibility over an arbitrary 1-D, 2-D or 3-D earth has not yet been fully investigated. Work has been carried out to estimate the physical and geometric parameters of some simple models. Ward (1959) described a method of determining the ratio of magnetic susceptibility of a conducting magnetic sphere to the susceptibility of the background rock. He used a uniform field for frequencies which span a large range but encompass the critical frequency at which the frequency-independent magnetic field cancels the in-phase component due to induced current. Fraser (1973) proposed a way to estimate the amount of magnetite contained in a vertical dyke under the assumption that the body is non-conductive. Fraser (1981) also developed a magnetite mapping technique for the horizontal coplanar coils of a closely coupled multi-coil airborne EM system. That technique yields contours of apparent weight per cent magnetite under the assumption that the conductivity of the Earth is represented by a homogeneous half-space.

In this paper we attack the inverse problem of the reconstruction of susceptibility by assuming that $\varepsilon = \varepsilon_0$ and that σ is variable, but known. We restrict ourselves to the 1-D problem. We begin with the expression for the forward-modelled data from a horizontal coplanar system over a 1-D earth. We next outline the inversion procedure and derive expressions for the sensitivities. Synthetic and field data are then inverted and we present summary comments in a concluding section.

THE FORWARD MODELLING

Consider two horizontal coils separated by a distance r as shown in Fig. 1. The transmitter is at height h_0 above the earth's surface and carries a harmonic current $I\,e^{i\omega t}$. The earth is characterized by a set of horizontal layers whose thickness, conductivity and suceptibility of the ith layer are given by $(h_i, \sigma_i, \kappa_i)$. In this paper we work with both magnetic permeability and susceptibility, which are related through the equation $\mu = \mu_0(1+\kappa)$, where μ_0 is the value of magnetic permeability in free space. The expression for the total magnetic field measured at the surface was given by Ryu, Morrison & Ward (1970). In the Hankel transform domain, and under the current coordinate system, the secondary electric field above the surface can be expressed as

$$E(\lambda, \omega, z_{\text{obs}}) = A \exp(-2u_0 h_0)\frac{Z^1 - Z_0}{Z^1 + Z_0}\exp(u_0 z_{\text{obs}}),$$
$$A = -\frac{i\omega\mu_0 a I J_1(\lambda a)}{2\mu_0}, \tag{1}$$

where λ is the Hankel transformation parameter and ω is the angular frequency. The input impedance in the first layer, Z^1,

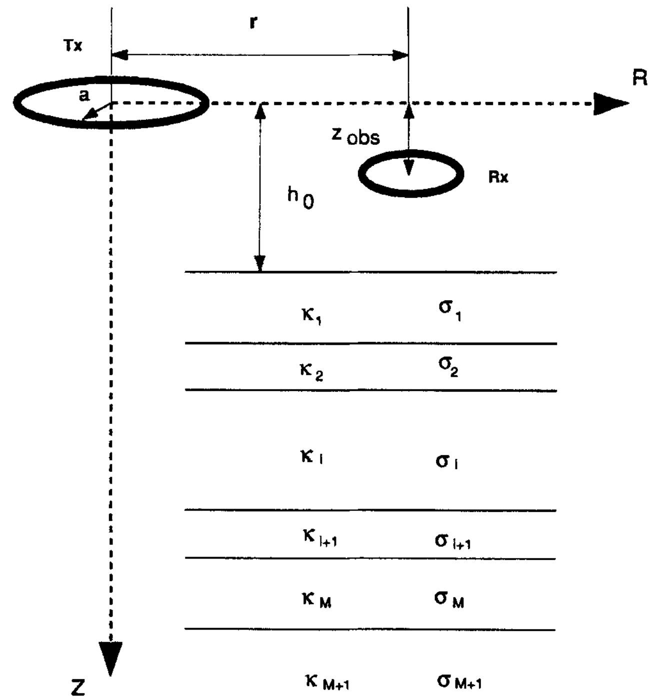

Figure 1. Geometry of the coplanar coil system. A horizontal loop of radius a is located at height h_0 above the surface of a 1-D earth. The source current has angular frequency ω and amplitude I. The receiver is situated at a radial distance r from the loop source.

can be found by the recursive formula (Ryu *et al.* 1970)

$$Z^i = Z_i\frac{Z^{i+1} + Z_i \tanh(u_i h_i)}{Z_i + Z^{i+1}\tanh(u_i h_i)}, \tag{2}$$

where the intrinsic impedance Z_i is given by

$$Z_i = -\frac{i\omega\mu_i}{u_i} \tag{3}$$

and

$$u_i^2 = \lambda^2 - \omega^2\varepsilon_0\mu_i + i\omega\sigma_i\mu_i. \tag{4}$$

In the half-space at the bottom there is no up-going wave and hence the input impedance is equal to the intrinsic impedance. That is, $Z^M = Z_M$. After inverse Hankel transformation, we obtain the secondary magnetic field in the frequency domain:

$$H_z(r, \omega, z_{\text{obs}}) = \frac{-1}{i\omega\mu_0}\int_0^\infty E(\lambda, \omega, z_{\text{obs}})\lambda^2 J_0(\lambda r)\,d\lambda. \tag{5}$$

The induced secondary voltage measured in a receiver coil is the time derivative of the magnetic flux and is expressed in the frequency domain as

$$V(r, \omega, z_{\text{obs}}) = -i\omega\mu_0\int_{DS} H_z(r, \omega, z_{\text{obs}})\,ds, \tag{6}$$

where DS is the effective area of the receiver. Field data sets take on different forms. The responses can be the secondary magnetic fields or voltage, or they can be total magnetic fields or voltage; these latter responses require the inclusion of the primary field. When secondary fields or voltages are used, the data are usually normalized by the primary field and provided in ppm. Responses in a field survey are acquired at a number of different frequencies and at each frequency both in-phase and quadrature phase (or real and imaginary) data can be obtained. The phase determination is made with respect to the primary magnetic field.

Due to magnetic polarization, the magnetic field retains a non-zero value when the frequency tends to zero. Let

$$\tilde{Z}_i = \lim_{\omega \to 0} \left(-\frac{\lambda}{i\omega} \right) Z_i = \mu_i, \tag{7}$$

be the normalized intrinsic impedance, and

$$\tilde{Z}^i = \lim_{\omega \to 0} \left(-\frac{\lambda}{i\omega} \right) Z^i = \mu_i \frac{\mu_{i+1} + \mu_i \tanh(\lambda h_i)}{\mu_i + \mu_{i+1} \tanh(\lambda h_i)} \tag{8}$$

be the normalized input impedance. The vertical magnetic field at zero frequency can then be expressed as

$$\lim_{\omega \to 0} H_z(r, \omega, z_{\text{obs}})$$
$$= aI \int_0^\infty \frac{\lambda(\tilde{Z}^1 - \mu_0)}{2(\tilde{Z}^1 + \mu_0)} \exp[\lambda(z_{\text{obs}} - 2h_0)] J_1(\lambda a) J_0(\lambda r)\, d\lambda. \tag{9}$$

If $\mu_i = \mu_0$, where $i = 1, 2, \dots, M$, then $\tilde{Z}^i = \mu_0$ and hence $H_z(\omega)$ will tend to zero when $\omega \to 0$. Conversely, if any one of the layers has non-zero susceptibility then the magnetic field will be non-zero. For a half-space with a conductivity σ and a magnetic permeability μ illuminated by a dipole of moment m, and with both source and receiver sitting at the same height h_0, the solution is reduced to

$$H_z = \frac{m}{4\pi} \left(\frac{\mu_1 - \mu_0}{\mu_0 + \mu_1} \right) \frac{8h_0^2 - r^2}{(4h_0^2 + r^2)^{2.5}}. \tag{10}$$

The derivation of the above result is given in Appendix A. Thus the induced static magnetic field due to a dipole located at h_0 above the surface is equal to that of an image dipole of strength $m(\mu_1 - \mu_0)/(\mu_1 - \mu_0)$ buried at a depth h_0 beneath the surface. This magnetic field is the same as that produced by effective magnetic charges on the surface of the half-space, where the susceptibility is discontinuous.

THE INVERSE ALGORITHM

In the non-linear inverse problem, we are provided with observations d_i^{obs}, $i = 1, N$, and an associated error estimate ε_i for each datum. We are supplied with a forward algorithm so that the ith datum can be written as $d_i = F_i(\kappa)$, with the understanding that the conductivity and permittivity are included in the forward mapping. The inverse problem is non-unique. We proceed in the usual manner by introducing a model objective function and then finding that model which minimizes the objective function subject to fitting the data. Because the magnetic susceptibilities of most minerals and rocks are positive, imposed positivity is requried in the inversion. An obvious way to achieve this would be the use of $\ln(\kappa)$ instead of κ as our model. Another means would be the introduction of a non-linear mapping $m = f(\kappa)$.

To be general, m is used as the model parameter in the following derivation. m could be κ, $\ln(\kappa)$ or $f(\kappa)$. Our model objective function,

$$\phi_{\text{m}} = \alpha \int w_s(z)(m - m_0)^2\, dz + (1 - \alpha) \int w_f(z) \left[\frac{\partial(m - m_0)}{\partial z} \right]^2 dz, \tag{11}$$

penalizes vertical roughness and differences between the recovered model and a reference model, m_0. In eq. (11) α is a parameter that controls the relative importance of the two terms, and w_s and w_f are weighting functions which can be prescribed by the user. When the earth is divided into layers of constant susceptibility, eq. (11) can be discretized and written as

$$\phi_{\text{m}} = \| W_{\text{m}}(m - m_0) \|^2, \tag{12}$$

where $m = (m_1, m_2, \dots m_M)^{\text{T}}$ is a model parameter vector and W_{m} is an $M \times M$ weighting matrix.

We chose a data misfit objective function

$$\phi_{\text{d}} = \| W_{\text{d}}(D^{\text{obs}} - D) \|^2 = \sum_{i=1}^{N} \left(\frac{d_i^{\text{obs}} - d_i}{\varepsilon_i} \right)^2, \tag{13}$$

where D^{obs} and D are the observed and predicted data, respectively, and ε_i is the standard deviation of the ith datum. Our goal is to find a model m that minimizes eq. (12) subject to the constraint that ϕ_{d} in eq. (13) is equal to a target misfit ϕ_{d}^*. If the errors are Gaussian and independent then ϕ_{d} is a chi-squared variable and its expected value is approximately equal to N for $N > 5$. Correspondingly, we often set $\phi_{\text{d}}^* \simeq N$. The optimization problem of minimizing eq. (12) subject to $\phi_{\text{d}} = \phi_{\text{d}}^*$ requires minimizing

$$\phi(m) = \phi_{\text{m}} + \beta^{-1}(\phi_{\text{d}} - \phi_{\text{d}}^*), \tag{14}$$

where β^{-1} is a Lagrange multiplier.

The optimization problem is non-linear and can be solved by linearizing and iterating to a solution. Let $m^{(n)}$ be the model at the nth iteration and let δm be a perturbation. The effect of the perturbation on the ith datum is given through a Taylor's expansion:

$$d_i[m^{(n)} + \delta m] \simeq F_i[m^{(n)}] + \sum_j \frac{\partial F_i}{\partial m_j} \delta m_j \equiv d_i^{(n)} + \sum_j J_{ij} \delta m_j, \tag{15}$$

where $J_{ij} = \partial d_i / \partial m_j$ is the sensitivity which indicates how d_i is affected by changing the model parameter for the jth layer. In order to keep excessive structure from entering the solution we reduce the misfit gradually. We choose the target misfit at the $(n+1)$th iteration as $\phi_{\text{d}}^{*(n+1)} = \gamma \phi_{\text{d}}^{(n)}$ where $\gamma < 1$. Our problem becomes: minimize

$$\phi = \| W_{\text{m}}[\delta m + m^{(n)} - m_0] \|^2$$
$$+ \beta^{-1} \{ \| W_{\text{d}} \{ D^{\text{obs}} - F[m^{(n)} + \delta m] \} \|^2 - \phi_{\text{d}}^{*(n+1)} \}. \tag{16}$$

Writing $F[m^{(n+1)}] = F[m^{(n)}] + J\delta m$ and setting the gradient $\nabla_{\delta m} \phi = 0$ we obtain

$$\delta m = [\beta W_{\text{m}}^{\text{T}} W_{\text{m}} + J^{\text{T}} W_{\text{d}}^{\text{T}} W_{\text{d}} J]^{-1}$$
$$\times \{ J^{\text{T}} W_{\text{d}}^{\text{T}} W_{\text{d}} \delta D_n + \beta W_{\text{m}}^{\text{T}} W_{\text{m}} [m_0 - m^{(n)}] \}, \tag{17}$$

where δD_n is

$$\delta D_n = D^{\text{obs}} - F[m^{(n)}]. \tag{18}$$

The selection of β is obtained in the manner outlined by Constable, Parker & Constable (1987). Let $\beta^{(n-1)}$ denote the accepted value of β from the $(n-1)$th iteration. Trial values of β opening a few orders of magnitude around $\beta^{(n-1)}$ are used to evaluate eq. (17). Forward modelling is performed on the updated trial models, and the misfit curve $\phi_{\text{d}}(\beta)$ is generated. We then find the β which generates the desired target misfit, or if that is not achievable, select that β which produces the minimum misfit. The inversion procedure continues until the

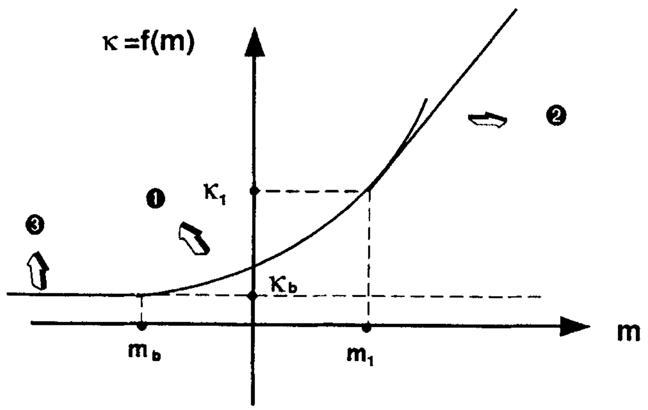

Figure 2. Non-linear mapping for positivity constraint. Segment 1 is an exponential function and segment 2 is a straight line whose slope equals 1. Segment 3 is a straight line parallel to the m-axis.

desired misfit is achieved and further iterations produce no significant reduction in the model objective function.

Positivity of the solution can be guaranteed in a number of ways. The simplest is to choose $m = \ln(\kappa)$ as the model. Since $\delta \ln(\kappa) = \delta\kappa/\kappa$, the sensitivities are easily obtained for this parameter. The difficulty with this mapping is that near-zero values carry too much weight in the model objective function, and large values of susceptibility are overestimated due to the nature of the logarithm function. To overcome these difficulties we define $m = f(\kappa)$ as a three-piece mapping in which $m = \kappa$ for κ greater than κ_1 and $m = m_b$ for $\kappa < \kappa_b$. An exponential function is used to represent susceptibility values between κ_b and κ_1. Fig. 2 shows the mapping. The forward and inverse mappings, $m = f(\kappa)$ and $\kappa = f^{-1}(m)$, are given by

$$m(\kappa) = \begin{cases} m_b & \kappa < \kappa_b \\ \kappa_1\left[\ln\left(\dfrac{\kappa}{\kappa_1}\right) + 1\right], & \kappa_b \le \kappa \le \kappa_1, \\ \kappa & \kappa > \kappa_1 \end{cases} \tag{19}$$

and

$$\kappa(m) = \begin{cases} m & m \ge m_1 \\ \kappa_1 \exp\left[\left(\dfrac{m}{\kappa_1} - 1\right)\right], & m_b < m < m_1, \\ \kappa_b & m \le m_b \end{cases} \tag{20}$$

where m_b is

$$m_b = \kappa_1\left[\ln\left(\frac{\kappa_b}{\kappa_1}\right) + 1\right]. \tag{21}$$

With this mapping the recovered susceptibility has a minimum value of κ_b but this is chosen small enough so that its effect on the data is insignificant compared to the errors on the observations.

CALCULATION OF SENSITIVITIES

The calculation of sensitivities $J_{ij} = \partial d_i/\partial m_j$ is an important part of the algorithm. Here we use the adjoint Green's function method. There are a number of choices for the data and for the definition of m, but all of the sensitivities can be obtained once $\partial E/\partial\mu$ is known. For instance, if the secondary fields are measured, the sensitivities for H_z are

$$\frac{\partial H_z(r, \omega, z_{obs})}{\partial m_i} = -\frac{1}{i\omega\mu_i}\int_0^\infty \frac{\partial E(\lambda, \omega, z_{obs})}{\partial m_i} J_0(\lambda r)\lambda^2\, d\lambda. \tag{22}$$

Because $\mu = \mu_0(1+\kappa)$ the sensitivity for any $m = f(\kappa)$ can be easily generated.

ADJOINT GREEN'S FUNCTION SOLUTION

The sensitivities can be computed using a modified adjoint Green's function solution. The basic equations for this problem are (Ryu 1970)

$$\begin{aligned} i\omega\mu H_r(r,\theta,z) &= \frac{\partial E_\theta(r,\theta,z)}{\partial z}, \\ i\omega\mu H_z(r,\theta,z) &= -\frac{1}{r}\left[\frac{\partial}{\partial r}(rE_\theta(r,\theta,z))\right], \\ \frac{\partial H_r(r,\theta,z)}{\partial z} - \frac{\partial H_z(r,\theta,z)}{\partial r} &= (i\omega\varepsilon_0 + \sigma)E_\theta(r,\theta,z) + I_s, \end{aligned} \tag{23}$$

where I_s is the source and r, θ and z are variables in the cylindrical coordinate system. Due to the symmetry of the problem, electric and magnetic fields are no longer functions of θ. For simplicity, we use E to denote E_θ. The permeability μ is a function of depth, and for our layered earth it is represented as

$$\mu(z) = \sum_{i=1}^{M} \mu_i\psi_i(z), \tag{24}$$

where M is the number of layers and $\psi_i(z)$ is the box car function, which is unity on the support of the ith layer and zero elsewhere. Substituting (24) into (23) and taking derivatives with respect to μ_i in each layer yields the partial differential equation for the sensitivity problem. In the Hankel transform domain, it is given by

$$\begin{aligned} \mathscr{L}\frac{\partial E(\lambda,\omega,z)}{\partial\mu_i} &= i\omega\psi_i(z)(i\omega\varepsilon_0 + \sigma)E(\lambda,\omega,z) \\ &\quad + \frac{1}{\mu_i}\frac{\partial E(\lambda,\omega,z)}{\partial z}[\delta(z - z_i) - \delta(z - z_{i+1})] \\ &\quad + i\omega\frac{\partial\mu}{\partial z}\frac{\partial H_r}{\partial\mu_i}, \end{aligned} \tag{25}$$

where the operator $\mathscr{L}$ is

$$\mathscr{L} = \frac{\partial^2}{\partial z^2} - u^2. \tag{26}$$

Detailed derivations of the above equation are given in Appendices B and C. A Green's function is introduced into the problem. Multiplying both sides of eq. (25) by the Green's function and integrating by parts we obtain

$$\begin{aligned} &\left(G\frac{\partial^2}{\partial z^2}\frac{\partial E}{\partial\mu_i} - \frac{\partial G}{\partial z}\frac{\partial}{\partial z}\frac{\partial E}{\partial\mu_i}\right)\Bigg|_{-\infty}^{\infty} + \int_{-\infty}^{\infty}\frac{\partial E}{\partial\mu_i}\left(\frac{\partial^2}{\partial z^2}G - u_i^2 G\right)dz \\ &= \int_{-\infty}^{\infty} i\omega\psi_i(z)(i\omega\varepsilon_0 + \sigma_i)GE\,dz - \frac{G}{\mu_i}\frac{\partial E}{\partial z}\Bigg|_{z_i}^{z_{i+1}}. \end{aligned} \tag{27}$$

The boundary term on the left-hand side vanishes because the electric field for any finite source tends to zero at infinity and so do its derivatives. Thus, if the Green's function satisfies the equation

$$\begin{aligned}
&\frac{\partial^2}{\partial z^2} G(\lambda, \omega, z) - u_i^2 G(\lambda, \omega, z) = \delta(z - z_{\mathrm{obs}}), \\
&G(\lambda, \omega, z)|_{z=z_i^-} = G(\lambda, \omega, z)|_{z=z_i^+}, \\
&G(\lambda, \omega, z) \to 0 \qquad \text{when} \quad |z| \to \infty,
\end{aligned} \tag{28}$$

then the sensitivity for the electric field is

$$\frac{\partial E(\lambda, \omega, z_{\mathrm{obs}})}{\partial \mu_i} = \int_{-\infty}^{\infty} i\omega\psi_i(z)(i\omega\varepsilon_0 + \sigma_i) G(\lambda, \omega, z) E(\lambda, \omega, z)\, dz - \frac{G(\lambda, \omega, z)}{\mu_i} \frac{\partial E(\lambda, \omega, z)}{\partial z}\Bigg|_{z_i}^{z_{i+1}}, \tag{29}$$

where E is the primary field in the ith layer and G the corresponding Green's function. The primary field is that produced by the transmitter, and the auxiliary field G is due to a vertical magnetic dipole with unit strength at the observing point z_{obs}. These fields are given by

$$\begin{aligned}
E_i(\lambda, \omega, z) &= A_i(\lambda, \omega) \exp[u_i(z - z_i)] + B_i(\lambda, \omega) \exp[-u_i(z - z_i)], \\
G_i(\lambda, \omega, z) &= a_i(\lambda, \omega) \exp[u_i(z - z_i)] + b_i(\lambda, \omega) \exp[-u_i(z - z_i)],
\end{aligned} \tag{30}$$

where the coefficients of the upgoing and downgoing waves are given by the following formulae:

$$\begin{aligned}
A_i(\lambda, \omega) &= B_i(\lambda, \omega) \exp[-2u_i h_i] \frac{Z^{i+1} - Z_i}{Z^{i+1} + Z_i}, \\
B_i(\lambda, \omega) &= B_{i-1}(\lambda, \omega) \exp[-u_{i-1} h_{i-1}] \frac{Z^i + Z_i}{Z^i + Z_{i-1}}, \\
a_i(\lambda, \omega) &= \frac{A_i(\lambda, \omega)}{i\omega\mu_i I a J_1(\lambda a)}, \\
b_i(\lambda, \omega) &= \frac{B_i(\lambda, \omega)}{i\omega\mu_i I a J_1(\lambda a)}, \\
B_0(\lambda, \omega) &= -\frac{i\omega\mu_0 a I J_1(\lambda a)}{2u_0}.
\end{aligned} \tag{31}$$

The input impedance and intrinsic impedance can be calculated by using eqs (2) and (3). For the convenience of computation, eq. (29) can be reorganized to (Appendix D)

$$\frac{\partial E(\lambda, \omega, z_{\mathrm{obs}})}{\partial \mu_i} = -\frac{2u_i^2}{\mu_i}\left[\int_{z_i}^{z_{i+1}} G(\lambda, \omega, z) E(\lambda. \omega, z)\, dz - 2A_i b_i h_i\right] + i\omega(i\omega\varepsilon_0 + \sigma_i) \int_{z_i}^{z_{i+1}} G(\lambda, \omega, z) E(\lambda, \omega, z)\, dz. \tag{32}$$

Appendix E outlines the detailed calculation of eq. (32). The sensitivities for the vertical component of the magnetic field are thus

$$\frac{\partial H_z(\lambda, \omega, z_{\mathrm{obs}})}{\partial \mu_i} = \int_0^{\infty} \frac{\partial E(\lambda, \omega, z_{\mathrm{obs}})}{\partial \mu_i} J_0(\lambda r) \lambda^2\, d\lambda = S_1 + S_2, \tag{33}$$

where

$$S_1 = -\frac{2iu_i^2}{\mu_i^2} \int_0^{\infty} \left[\int_{z_i}^{z_{i+1}} G(\lambda, \omega, z) \frac{E(\lambda, \omega, z)}{\omega}\, dz - 2\frac{A_i(\lambda, \omega, h_i)}{\omega} b_i h_i\right] J_0(\lambda r) \lambda^2\, d\lambda, \tag{34}$$

and

$$S_2 = -(i\omega\varepsilon_0 + \sigma_i) \int_0^{\infty} \left[\int_{z_j}^{z_{j+1}} G(\lambda, \omega, z) E(\lambda, \omega, z)\, dz\right] \times J_0(\lambda r) \lambda^2\, d\lambda. \tag{35}$$

Like the magnetic field, the sensitivities also retain a non-zero value when frequency tends to zero. From eqs (7) and (8), the input and intrinsic impedances, after being normalized by $i\omega$, asymptote to a constant when frequency tends to zero. Consequently, the coefficients a_i and b_i are proportional to ω^0, and A_i and B_i are proportional to ω^1 when $\omega \to 0$. That in turn means that $G \propto \omega^0$ and $E \propto \omega^1$ when $\omega \to 0$. Therefore, the first term S_1 in eq. (33), which represents the influence of sources on the two boundaries of each layer, will not tend to zero at zero frequency. The second term S_2, on the other hand, will tend to zero when the frequency tends to zero. The two boundary sources in the calculation of sensitivities can be viewed as layers of magnetic charges. Those surface magnetic charges are due to the sudden change of susceptibility on boundaries and they remain as the frequency goes to zero. As frequency increases, eddy currents will become stronger, and this adds a frequency-dependent term to the sensitivities.

A numerical example of the sensitivities for horizontal coplanar coils with a coil separation of 10 m and at height 30 m above a half-space of 10^{-2} S m^{-1} and a magnetic susceptibility of 0.1 SI units is given in Fig. 3. Panels (a) and (b) show how the amplitudes of real and imaginary components of the sensitivities vary with respect to frequency. At low frequency the real component remains at a constant value due to magnetic polarization. As frequency increases, the induced currents become stronger and the real component of the sensitivities become frequency-dependent. At a certain frequency, in this case around 10^3 Hz, the frequency-dependent term begins to dominate. For a given susceptibility structure the transition frequency lowers as conductivity increases. The imaginary component, on the other hand, is completely frequency-dependent. At low frequency, magnetic dipoles change orientation almost synchronously with the primary field, therefore the amplitude of the imaginary component of the sensitivities is very small. Below 1000 Hz the amplitude increases linearly with frequency. It then increases non-linearly and reaches a maximum around 10 000 Hz.

Both components of the sensitivities also behave differently with depth. The real component begins at a constant value and decreases with depth, but for the imaginary part there is a depth at which the sensitivity is maximized. This characteristic contributes greatly to the depth resolution obtained in the inversion. Fig. 3(c) presents the absolute value of the frequency-independent part of the sensitivities as a function of depth and coil separation. When the coil separation is much smaller than the observation height, as in the case of this example, this term generally decreases with depth. The frequency-dependent term of the real component of the sensitivities is obtained by subtracting the frequency-independent term from

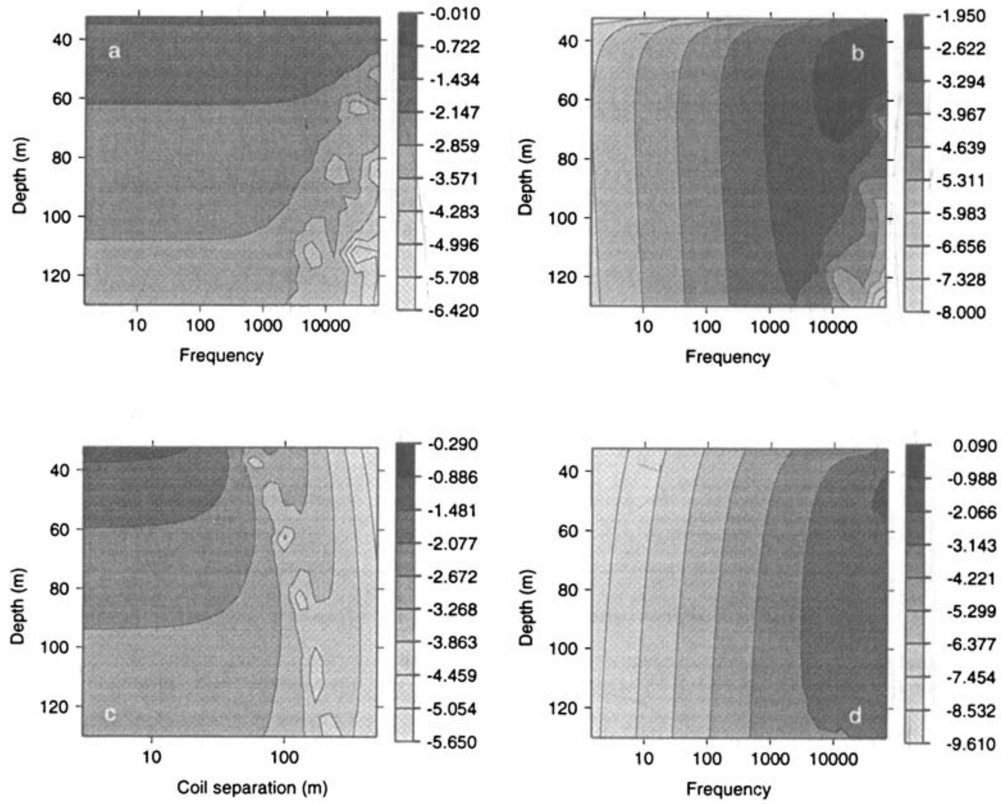

Figure 3. The absolute value of sensitivities (in logarithmic scale) over a half-space. The conductivity is 0.01 S m^{-1} and the susceptibility is 0.1 SI units. The data were calculated for a coil separation of 10 m and survey height of 30 m. (a) Real component of the sensitivities; (b) imaginary component of the sensitivities; (c) frequency-independent term in the real component of the sensitivities; (d) frequency-dependent term in the real component of the sensitivities.

Fig. 3(a). Fig. 3(d) shows the result for a source–receiver separation of 10 m. It is similar to the imaginary component of the sensitivities in that at frequencies higher than 1000 Hz it also reaches a maximum at depth. At frequencies lower than 1000 Hz, the amplitude of the frequency-independent component of the sensitivities is linear with frequency. However, the amplitude of the frequency-dependent sensitivity is much smaller than the frequency-independent component; thus, during an inversion, the frequency-independent component of the in-phase part of the sensitivities may limit depth resolution.

EXAMPLES

For all the synthetic data in this section we assume a coplanar system with a coil separation of 10 m in which the transmitter has unit area and carries a harmonic electric current of 1 Amp. The earth is divided into 44 layers and the thicknesses of the layers increase with depth to compensate for the loss of resolution. The conductivity structure is assumed known and the mapping parameters κ_b and κ_1 are fixed at 10^{-6} and 10^{-3} SI units.

As a first example, we invert data from a ground system that is 0.5 m above the surface. The data are calculated at 10 frequencies; 110, 220, 440, 880, 1760, 3520, 7040, 14 080, 28 160 and 56 320 Hz and contaminated with 24 per cent Gaussian noise. The model parameter used in this inversion is related to κ through the non-linear mapping given by eq. (19). Parameter α in eq. (11) is set to 0.02. The starting and reference susceptibility models were half-spaces of values 0.0 and 10^{-6} SI, respectively. The parameter γ was chosen as 5. The results are shown in Fig. 4. After seven iterations the inversion converged to the desired target misfit of 20. Fig. 4(a) shows the true conductivity structure and Fig. 4(b) shows the reconstructed and true susceptibility models. Figs 4(c) and (d) show the misfit curve and model norm as functions of the number of iterations. The inversion has recovered a very good representation of the true susceptibility structure.

In a second example, whose results are given in Fig. 5, we invert data from a typical airborne survey in which in-phase and quadrature phase data at frequencies 900, 7200 and 56 000 Hz were collected at a flight height of 30 m. The data were contaminated with 0.5 per cent Gaussian noise. Starting and reference models in this example were 0.02 and 10^{-6} SI, respectively. The true conductivity model, given in Fig. 5(c), is assumed known. We first used the logarithm of susceptibility as the model parameter. The reconstructed model, obtained after seven iterations, fits the data to the desired level, but overshoots the true model. This is primarily the result of using $\ln(\kappa)$ as a model parameter. Using the non-linear mapping (eq. 19) to guarantee positivity yields the model in Fig. 5(b). This model is a better representation of the true model and was obtained in four iterations. In both cases, the inversion converged to the desired target misfit of 6. Plots of the data misfits for both inversions are provided in Fig. 5(d). In carrying out the inversion, parameters α and γ were chosen to be the same as those in the previous example.

The primary contribution to the EM responses is from eddy currents induced in the earth, and the magnitude of the data

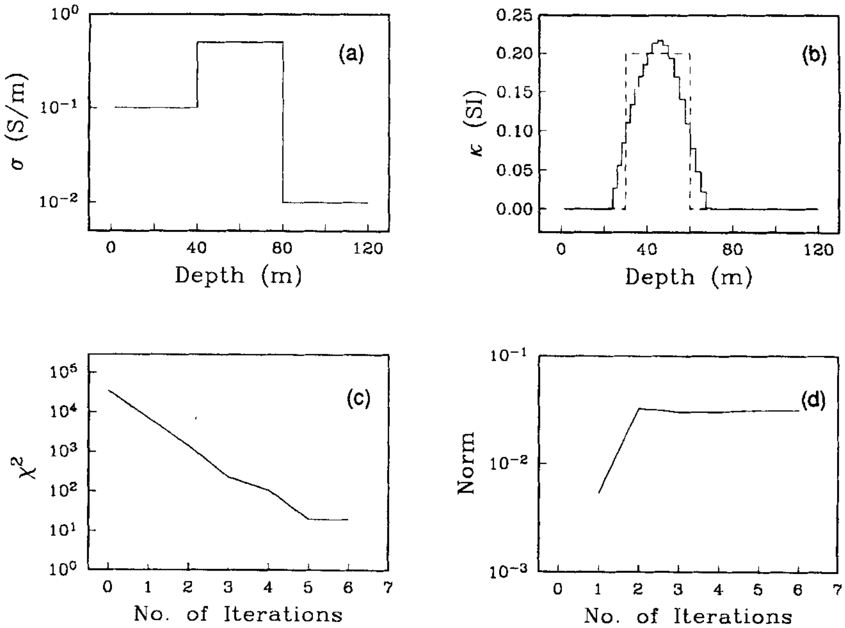

Figure 4. Inversion of ground system data. (a) The conductivity structure used in the inversion. Its value below 80 m is 0.01 S m^{-1}. (b) Recovered (solid line) and true susceptibility models (dashed line). (c) Misfit curve for the inversion. (d) Model norm as a function of iteration.

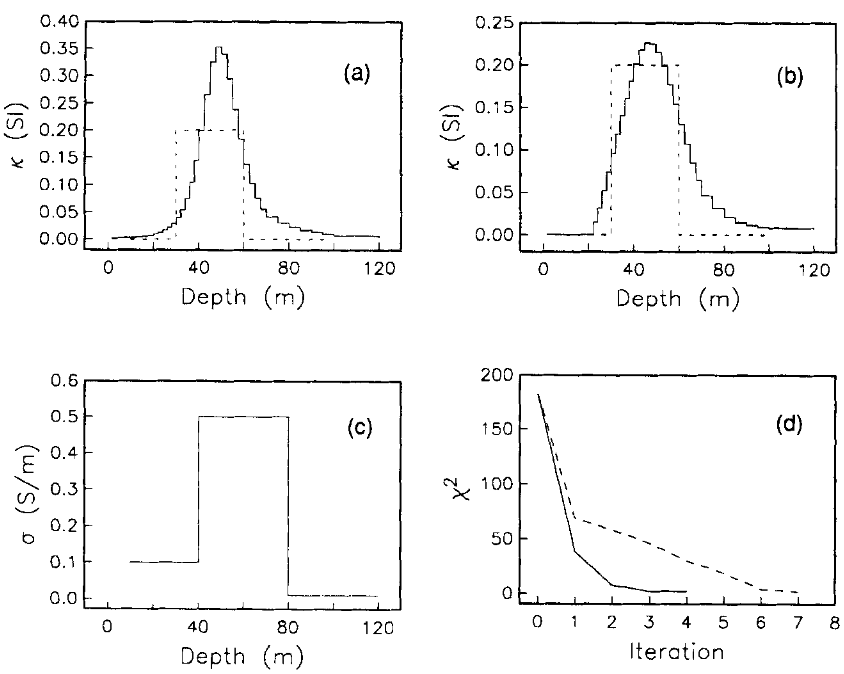

Figure 5. Inversion with correct knowledge of conductivity structure. (a) Recovered (solid line) and true susceptibility models (dashed line) from the inversion in which ln(κ) was used as the model parameter. (b) The result of the inversion which uses the three-piece non-linear mapping for the model parameters. The solid line denotes the recovered model and the dashed line denotes the true model. (c) The true conductivity structure. (d) The convergence curves for inversion with the non-linear mapping (solid line) and inversion with ln(κ) as the model parameter (dashed line).

is dependent upon the electrical conductivity structure. It follows that inversions for susceptibility which are performed with incorrect knowledge of the electrical conductivity will suffer some deterioration. We illustrate this by repeating the last inversion but this time using an approximate conductivity model. The conductivity model is obtained by using a separate inversion algorithm which recovers a 1-D electrical structure from horizontal loop EM data by assuming that μ and ε take their values in the air. The algorithm was terminated after the second iteration when the misfit was 75.4, well above the desired value of 6. The true and the approximate conductivity models are shown in Fig. 6(a). Now we use the approximate conductivity and invert for κ. The algorithm plateaued to a minimum misfit of about $\phi_d = 28$ after nine iterations. The recovered susceptibility in Fig. 6(b) shows increased susceptibility at about the right depth, but it overshoots the true model

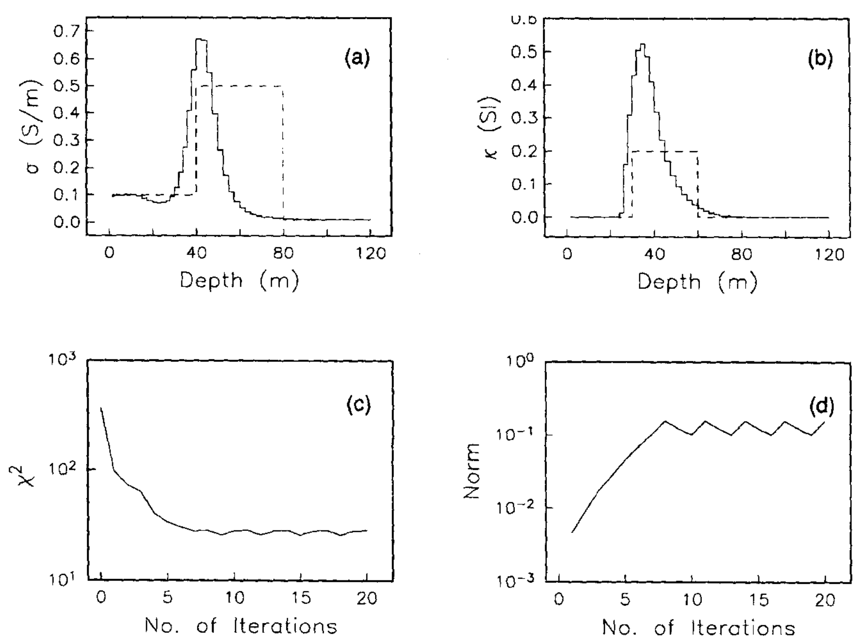

Figure 6. Effect of incorrect knowledge of the conductivity distribution on the inversion. (a) Solid line denotes the approximate conductivity model and dashed line denotes the true model. (b) The resultant susceptibilty model (solid line) and the true model (dashed line). (c) The misfit curve for the inversion. (d) The model norm as a function of iteration.

significantly and is not an accurate representation of the true model. This discrepancy increases as the conductivity model becomes a poorer representation of the true conductivity.

As a field example we now invert airborne EM data acquired at Mt Milligan, which is a Cu–Au porphyry deposit located in central British Columbia, Canada. The in-phase and quadrature phase data at frequencies of 900, 7200 and 56 000 Hz were taken about every 10 m along the flight line. The coil separation is 8.0 m for 900 and 7200 Hz data and 6.3 m for data at 56 000 Hz. The DIGHEM system was flown in north–south lines 100 m apart. Even though the flight lines are north–south we invert data at 13 stations along an east–west line (Y9600). This is because DC resistivity data were collected on east–west lines and they have been inverted by Oldenburg, Li & Ellis (1997). We will use their 2-D conductivity model in our susceptibility inversion. The DIGHEM data for the 13 stations are given in Fig. 7. The real component of the vertical component of the magnetic field at 900 Hz is negative at most of the stations. There are also some negative in-phase data at 7200 Hz. For airborne electromagnetic surveys, the negative in-phase data is a direct result of magnetization. For such surveys, the flight height h_0 is generally much greater than the coil separation r, and therefore the secondary magnetic field recorded at the receiver opposes the primary field. At low induction numbers the magnetic field due to magnetic charges at boundaries of susceptibility discontinuity can exceed the secondary fields generated by eddy currents in the Earth, and since they oppose each other, it is possible for the in-phase portion of the airborne EM response to be negative. At higher induction numbers, however, the effect of eddy currents will dominate.

In performing the inversion the Earth is divided into 22 layers, which is the same as the number of layers used in the inversion of the 2-D DC data. A contoured representation of that conductivity model is shown in Fig. 8(a). The laterally averaged conductivity beneath each station was used as a 1-D background conductivity for the susceptibility inversion. The model objective function was that given in eq. (14) with the parameter α set to 0.02. The model parameter $m(\kappa)$ for the inversion is connected to susceptibility through the non-linear mapping given in eq. (19). The mapping parameters κ_b and κ_1 were set to be 10^{-6} and 10^{-3} SI, respectively. The starting model for inversions at all the stations was a half-space of 0.02 SI. The reference model was a half-space of 10^{-6} SI.

The noise level in the data is assumed to be 10 per cent of the amplitude of the data. This resulted in a minimum standard deviation of less than 1 ppm for some data and is likely to have been overly optimistic. The cumulative initial chi-squared misfit for the 13 stations was 417 206. The result of the inversion is shown in Fig. 8(b), and the cumulative misfit has been reduced to 1795. Three regions of high susceptibility are observed in the upper 200 m and the maximum susceptibility is 0.1 SI. This result can be compared with Fig. 8(c), which shows the magnetite concentration provided by DeLong *et al.* (1991), which was visually estimated from borehole samples over the same section. Topography information is incorporated in Fig. 8(c). The larger magnetic anomaly in the centre is supported by four observations. The highest value in this anomaly is 8 per cent and the magnetite contents for the three other supporting points are 5 per cent. The high susceptibility at station 12.9 km in Fig. 8(b) corresponds well, both vertically and horizontally, with the borehole information. There is an indication in Fig. 8(c) of an enhanced magnetite content near 13.1 km and another more elongated concentration near 12.9 km. These are not pronounced features, but they do correlate with the inversion result in Fig. 8(b). The data from a ground magnetic survey at Mt Milligan have been inverted to recover a 3-D model of susceptibility (Li & Oldenburg 1996). The cross-section from the recovered 3-D susceptibility model is presented in Fig. 8(d). Three concentrations of susceptibility are observed, with the largest amplitude of 0.047 SI occurring at 12.7 km and at a depth of 200 m. This is

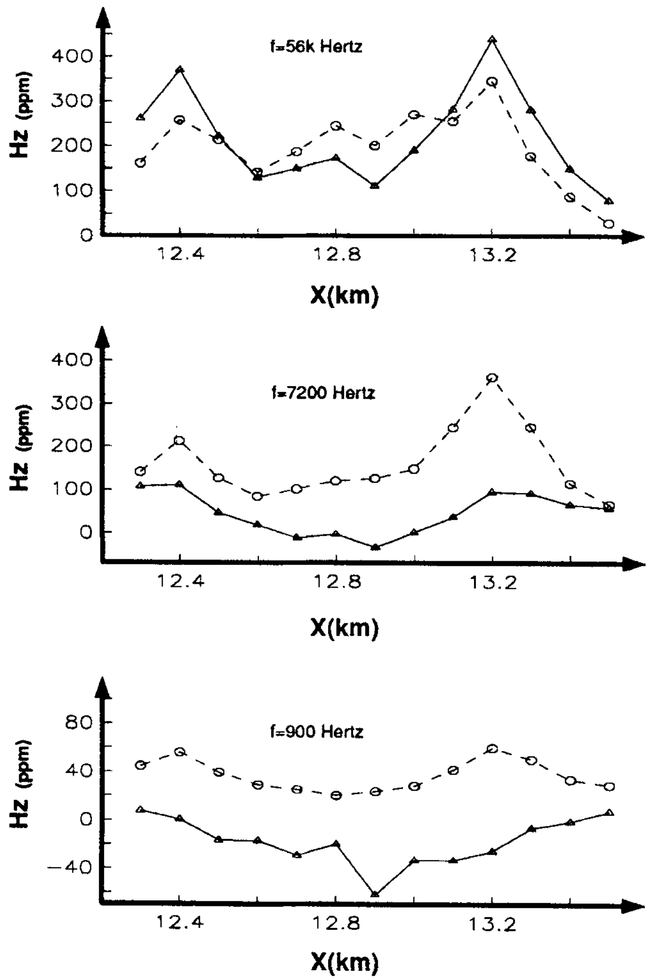

Figure 7. DIGHEM data from Mt Milligan, at section Y9600. The real component is denoted by the solid line and the imaginary component is denoted by the dashed line. The flight height varies between 25.2 and 48.8 m. The coil separation is 7.98 m at 900 and 7200 Hz, and 6.33 m at 56 000 Hz.

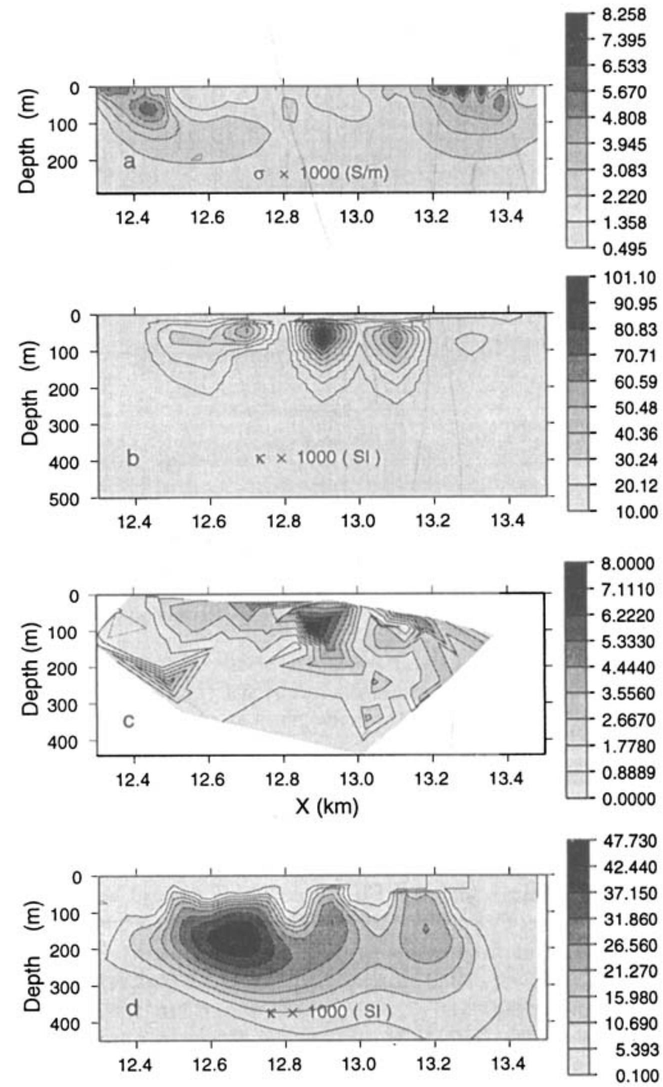

Figure 8. Inversion of DIGHEM data from Mt Milligan, section Y9600. (a) Recovered conductivity model from the inversion of 2-D DC data. (b) Susceptibility model reconstructed from the 1-D inversion of DIGHEM data. (c) Magnetite content in percentage from borehole information. (d) Susceptibility model from the 3-D inversion of static magnetic data.

considerably deeper than the susceptibility recovered by inverting the airborne EM data. Figs 8(b) and (d) both indicate high susceptibility at 12.7 km, but there is a lateral difference of about 100 m between the locations of the right-most anomaly. With the exception of this lateral shift in the right-hand anomaly, the greatest discrepancies between the models exist in the vertical direction. One possible explanation is that the depth of investigation, which is primarily controlled by skin depth and geometry, is less than 150 m in this case. Therefore, the airborne EM data are primarily sensitive to structure in the top 150 m, and structure with susceptibility lower than 0.1 SI and deeper than 200 m will not greatly affect the data. This has been confirmed by forward modelling.

Another possibility for the disagreement between Figs 8(b) and (d) is due to non-uniqueness in the inversion. The recovered model from the inversion of static magnetic data seems deeper and more spread out. Since the depth distribution in the 3-D model is a consequence of the depth weighting in the objective function, inappropriate design or use of that weighting function may affect the inversion. On the other hand, the quality of the results of the 1-D susceptibility inversion can be affected by 3-D variations in conductivity and susceptibility, which surely exist at Mt Milligan, and by incorrect estimation of the background conductivity. Ideally, we would like to incorporate the 3-D effects into the errors ascribed to the data, but we do not know how large these are. In the inversion in Fig. 8(b) we assigned a constant percentage error. Other reasonable errors schemes are: (1) constant base level plus a percentage of the data; (2) a fixed but different value for each frequency; and (3) uniform errors on all data. For a given data set, the inverted model depends upon the assigned errors and how well the data are misfit. To investigate this variability we carried out the inversions with different error schemes and additionally imposed a reasonable upper limit of 0.1 SI units on the recovered susceptibility. In Fig. 9(a) we show the inversion result when the standard deviation for data at 900, 7200 and 56 000 Hz is 5 ppm plus 10 per cent of the strength of the data. For Fig. 9(b) the standard deviations were 1, 4 and 10 ppm for data at the three respective frequencies, and in Fig. 9(c) the

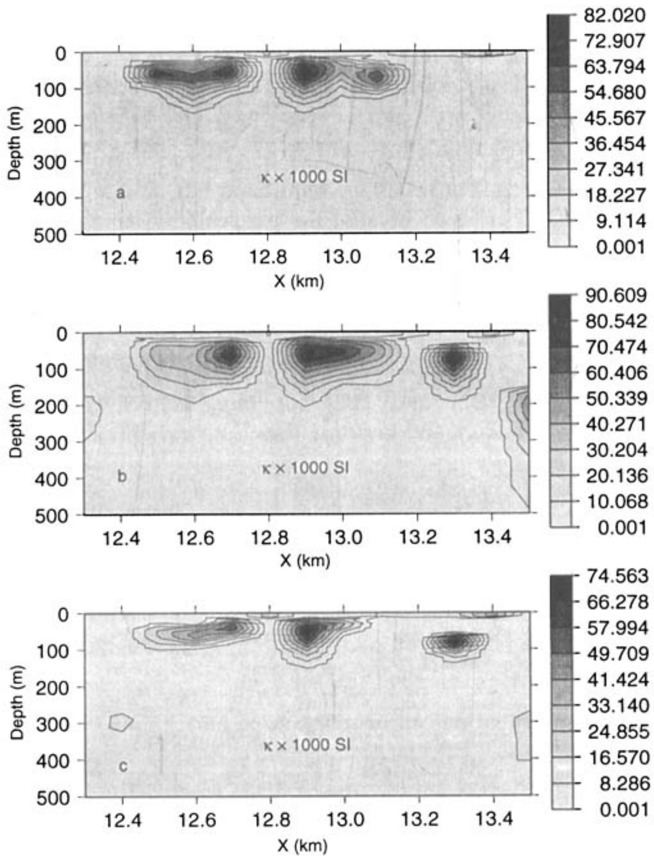

Figure 9. Recovered susceptibilty models from inversions with different error schemes: (a) the recovered model when the standard deviations were 5 ppm plus 10 per cent of the strength of the data; (b) the standard deviations were 1.4 and 10 ppm for data at 900, 7200 and 56 000 Hertz; and (c) a constant standard deviation of 10 ppm was used for all the data.

standard deviation for each datum was 10 ppm. There are differences between the three sections but they all identify anomaly highs at 12.6 km and 12.9 km. All susceptibility highs are concentrated within the top 150 m. This provides confidence that the algorithm is producing meaningful results.

CONCLUSIONS

The work presented here shows how electromagnetic data from a horizontal coplanar loop can be inverted to recover a 1-D susceptibility structure under the assumption that the electrical conductivity is known. Since the strength of induced magnetization inside the Earth depends upon the amplitude of the existing magnetic field, it follows that EM data at different frequencies are sensitive to susceptibilities at different depths. This is in contrast to static magnetic field data acquired on usual surveys. Our algorithm follows traditional inversion methodologies for solving underdetermined non-linear inverse problems and minimizes an objective function subject to fitting the data. Positivity is incorporated by using $\ln(\kappa)$ or a non-linear mapping of susceptibility as model parameters. Synthetic inversions indicate that convergence with the non-linear mapping usually requires fewer iterations to achieve the same misfit and generally produces a better representation of the true model. For field data, when using a 1-D inversion algorithm in complex environments, one is faced with the ubiquitous problem of specifying the observational errors and deciding how well the data should be fitted. This remains problematic but in our examples we used a variety of error assignments and imposed an upper limit on the constructed susceptibilities. The resultant images had common features and the main feature coincided with a region of high magnetite content inferred from visual estimates of borehole logs.

Reasonably accurate information about background conductivity is important for the inversion. If the true conductivity is known, the inversion can produce a good representation of the true magnetic susceptibility. However, when the conductivity is not accurate, the recovered susceptibility model will be distorted. This invites the challenge of carrying out simultaneous inversion of conductivity and susceptibility.

The method outlined in this paper is qualitatively useful. When accurate information about conductivity structure is available from other geophysical surveys such as DC resistivity surveys, our method may provide useful information about susceptibility structure. It can also be used in resistive environments where the effect of conductivity on the data is relatively small. For instance, this method is potentially useful for mapping titanomagnetites since these often occur in fairly resistive rocks. In general, however, simultaneous inversions are needed to recover conductivity and susceptibilty, and this paper has laid the theoretical foundation for such an inversion.

ACKNOWLEDGMENTS

This research was supported by an NSERC IOR grant and an industry consortium 'Joint and Cooperative Inversion of Geophysical and Geological Data'. The following companies are part of this consortium: Placer Dome, BHP Minerals, Noranda Exploration, Cominco Exploration, Falconbridge, INCO Exploration & Technical Services, Hudson Bay Exploration & Development, Kennecott Exploration Company, Newmount Gold Company, Western Mining Corporation and CRA Exploration Pty.

REFERENCES

Bhattacharyya, B.K., 1980. A generalized multibody model for inversion of magnetic anomalies, *Geophysics,* **45,** 255–270.

Constable, S.C., Parker, R.L. & Constable, C.G., 1987. Occam's inversion: A practical algorithm for generating smooth models from electromagnetic sounding data, *Geophysics,* **52,** 289–300.

DeLong, R.C., Godwin, E.I., Harris, M.H., Caira, N.M. & Rebagliati, C.M., 1991. Geology and alteration at the Mountain Milligan gold-porphyry deposit, central British Columbia, in *Geological Fieldwork 1990,* pp. 199–205, British Columbia Ministry of Energy, Mines and Petroleum Resources-Geological Survey Branch, Paper 1991-1.

Fraser, D.C., 1973. Magnetite ore tonnage estimates from an aerial electromagnetic survey, *Geoexploration,* **11,** 97–105.

Fraser, D.C., 1981. Magnetite with a multicoil airborne electromagnetic system, *Geophysics,* **46,** 1579–1593.

Gradshteyn, S., Ryzhik, I.M., 1965. *Table of Integrals, Series, and Products,* 4th edn, Academic Press Inc, New York, NY.

Guillen, A. & Menichetti, V., 1984. Gravity and magnetic inversion with minimization of a special functional, *Geophysics,* **49,** 1354–1360.

Keller, G.V., 1990. Rock and Mineral Properties, in *Electromagnetic Methods in Applied Geophysics: Investigations in geophysics,* Vol. 3, pp. 13–51, ed. Nabighian, M.N., Soc. Expl. Geophys., Tulsa, OK.

Last, B.J. & Kubik, K., 1983. Compact gravity inversion, *Geophysics,* **48,** 713–721.

Li, Y. & Oldenburg, D.W., 1996. 3-D inversion of magnetic data, *Geophysics,* **62,** 394–408.
Oldenburg, D.W., Li, Y. & Ellis, R.G., 1997. Inversion of geophysical data over a copper gold porphyry deposit: a case history for Mt Milligan, *Geophysics* (in press).
Ryu, J., Morrison, F.H. & Ward, S.H., 1970. Electromagnetic fields about a loop source of current, *Geophysics,* **35,** 862–896.
Wang, X. & Hansen, R.O., 1990. Inversion for magnetic anomalies of arbitrary three-dimensional bodies, *Geophysics,* **55,** 1321–1326.
Ward, S.H., 1959. Unique determination of conductivity, susceptibility, size, and depth in multifrequency electromagnetic exploration, *Geophysics,* **24,** 531–546.
Zeyen, H. & Pous, J., 1991. A new 3-D inversion algorithm for magnetic total field anomalies, *Geophys. J. Int.,* **104,** 583–591.

APPENDIX A: ZERO-FREQUENCY SOLUTION FOR H_z OVER A HALF-SPACE

The asymptotic expression for the vertical component of the magnetic field due to a dipole source of moment m, over a general 1-D earth at zero frequency is given by

$$\lim_{\omega\to 0} H_z(r,\omega,z_{\text{obs}}) = \frac{m}{4\pi}\int_0^\infty \frac{(\tilde{Z}^1-\mu_0)}{(\tilde{Z}^1+\mu_0)}\lambda^2 \exp[\lambda(z_{\text{obs}}-h_0)]J_0(\lambda r)\,d\lambda\,. \tag{A1}$$

For a half-space of $\mu=\mu_1$ and $\sigma=\sigma_1$, the input impedance equals the intrinsic impedance:

$$Z^1 = Z_1 = -\frac{i\omega\mu_1}{\sqrt{\lambda^2-\omega^2\varepsilon_0\mu_1+i\omega\mu_1\sigma_1}}\,. \tag{A2}$$

When the frequency tends to zero, the normalized input impedance is

$$\tilde{Z}^1 = \frac{\lambda}{-i\omega}\left(\frac{-i\omega\mu_1}{\lambda}\right) = \mu_1\,. \tag{A3}$$

Thus expression (A1) can be further reduced to

$$\lim_{\omega\to 0} H_z(r,\omega,z_{\text{obs}}) = \frac{m}{4\pi}\frac{(\mu_1-\mu_0)}{(\mu_1+\mu_0)}\int_0^\infty \lambda^2 \exp[\lambda(z_{\text{obs}}-2h_0)]J_0(\lambda r)\,d\lambda\,. \tag{A4}$$

From Gradshteyn & Ryzhik (1965, p. 712),

$$\int_0^\infty x^{m+1}\exp(-ax)J_v(bx)\,dx = (-1)^{m+1}b^{-v}\frac{d^{m+1}}{da^{m+1}}\left[\frac{(\sqrt{a^2+b^2}-a)^v}{\sqrt{a^2+b^2}}\right]. \tag{A5}$$

Letting $m=1$, $b=r$, $v=0$, $a=2h_0$ and $z_{\text{obs}}=0$ yields

$$\lim_{\omega\to 0} H_z(r,\omega,z_{\text{obs}}) = \frac{m(\mu_1-\mu_0)}{4\pi(\mu_1+\mu_0)}\frac{8h_0^2-r^2}{(4h_0^2+r^2)^{2.5}}\,. \tag{A6}$$

APPENDIX B: ADJOINT GREEN'S FUNCTION SOLUTION FOR THE SENSITIVITIES

From the first two expressions in eq. (23) we obtain

$$\frac{\partial^2}{\partial z^2}\frac{\partial E}{\partial \mu_i} = i\omega\mu\frac{\partial}{\partial z}\frac{\partial H_r}{\partial \mu_i} + i\omega\frac{\partial \mu}{\partial z}\frac{\partial H_r}{\partial \mu_i} + i\omega\frac{\partial H_r}{\partial z}\psi_i + i\omega H_r\frac{\partial \psi_i}{\partial z} \tag{B1}$$

and

$$-\frac{\partial}{\partial r}\left\{\frac{1}{r}\left[\frac{\partial}{\partial r}\left(r\frac{\partial E}{\partial \mu_i}\right)\right]\right\} = i\omega\mu\frac{\partial}{\partial r}\frac{\partial H_z}{\partial \mu_i} + i\omega H_z\frac{\partial \psi_i}{\partial r} + i\omega\frac{\partial H_z}{\partial r}\psi_i\,. \tag{B2}$$

Note that second terms on the right-hand side of both eq. (B1) and eq. (B2) are zero because the permeability in each layer remains constant and ψ_i is only a function of z. Multiplying both sides of the third expression in (23) with $i\omega\mu$, we obtain

$$i\omega\mu\frac{\partial}{\partial z}\frac{\partial H_r}{\partial \mu_i} - i\omega\mu\frac{\partial}{\partial r}\frac{\partial H_z}{\partial \mu_i} = (-\omega^2\mu\varepsilon_0 + i\omega\mu\sigma)\frac{\partial E}{\partial \mu_i}\,. \tag{B3}$$

Solving eqs (B1) and (B2) for $i\omega\mu(\partial/\partial z)(\partial H_r/\partial\mu_i)$ and $i\omega\mu(\partial/\partial r)(\partial H_z/\partial\mu_i)$, and inserting these into eq. (B3) leads to

$$\left[\frac{\partial^2}{\partial z^2}\frac{\partial E}{\partial \mu_i} - \left(i\omega H_r\frac{\partial \psi_i}{\partial z} + i\omega\psi_i\frac{\partial H_r}{\partial \mu_i}\right)\right] + \frac{\partial}{\partial r}\left\{\frac{1}{r}\left[\frac{\partial}{\partial r}\left(r\frac{\partial E}{\partial \mu_i}\right)\right] + i\omega\frac{\partial H_z}{\partial r}\psi_i\right\} = (-\omega^2\mu_i\varepsilon_0 + i\omega\sigma_i)\frac{\partial E}{\partial \mu_i}\,. \tag{B4}$$

The above equation can be reorganized into

$$\frac{\partial^2}{\partial z^2}\frac{\partial E}{\partial \mu_i} - \frac{\partial}{\partial r}\left\{-\frac{1}{r}\left[\frac{\partial}{\partial r}\left(r\frac{\partial E}{\partial \mu_i}\right)\right]\right\} - (-\omega^2\mu\varepsilon_0 + i\omega\sigma)\frac{\partial E}{\partial \mu_i} = i\omega\psi_i\left(\frac{\partial H_r}{\partial z} - \frac{\partial H_z}{\partial r}\right) + i\omega H_r\frac{\partial \psi_i}{\partial z}\,. \tag{B5}$$

Since there is no artificial source in the ith layer,

$$\frac{\partial H_r}{\partial z} - \frac{\partial H_z}{\partial r} = (i\omega\varepsilon_0 + \sigma)E\,, \tag{B6}$$

hence the sensitivity problem can be expressed as

$$\frac{\partial^2}{\partial z^2}\frac{\partial E}{\partial \mu_i} - \frac{\partial}{\partial r}\left\{-\frac{1}{r}\left[\frac{\partial}{\partial r}\left(r\frac{\partial E}{\partial \mu_i}\right)\right]\right\} - (-\omega^2\mu\varepsilon_0 + i\omega\sigma)\frac{\partial E}{\partial \mu_i} = (i\omega\psi_i(i\omega\varepsilon_0 + \sigma)E + i\omega H_r\frac{\partial \psi_i}{\partial z}\,. \tag{B7}$$

Since the box car basis function is actually the difference between two Heaviside functions, $\psi_i = \mathrm{H}(z-z_i) - \mathrm{H}(z-z_{i+1})$, the derivative of the box car with respect to depth is

$$\frac{\partial \psi_i}{\partial z} = \delta(z-z_i) - \delta(z-z_{i+1})\,. \tag{B8}$$

Due to its symmetry, this problem can be converted into the Hankel domain (Appendix C):

$$\frac{\partial^2}{\partial z^2}\frac{\partial E}{\partial \mu_i} - u^2\frac{\partial E}{\partial \mu_i} = i\omega\psi_i(i\omega\varepsilon_0 + \sigma)E + \frac{1}{\mu_i}\frac{\partial E}{\partial z}[\delta(z-z_i) - \delta(z-z_{i+1})]\,, \tag{B9}$$

where $u^2 = \lambda_2 - \omega^2\mu\varepsilon_0 + i\omega\mu\sigma$. Compared with the partial differential equation for the sensitivity of conductivity, this sensitivity problem has two extra terms located at the upper and lower boundaries of each layer. We solve eq. (B9) by introducing a Green's function G. Multiply both sides of eq. (B9) by G and integrate over the whole domain to obtain eq. (27). The boundary term on the left-hand side vanishes because the electric field for any finite source tends to zero at infinity and so do its derivatives. Thus, if the Green's function satisfies eq. (28) then the sensitivity for the electric field is given by eq. (29).

APPENDIX C: HANKEL TRANSFORMATION FOR EQ. (B7)

The Hankel transform is defined as

$$f(\lambda) = \int_0^\infty F(r) r J_1(\lambda r)\,dr\,. \tag{C1}$$

We want to take the Hankel transform of eq. (B7). Concentrating upon the second term, we have

$$\int_0^\infty \frac{\partial}{\partial r}\left\{\frac{1}{r}\left[\frac{\partial}{\partial r}\left(r\frac{\partial E}{\mu_i}\right)\right]\right\} r J_1(\lambda r)\,dr$$
$$= \int_0^\infty \left(r\frac{\partial^2}{\partial r^2}\frac{\partial E}{\partial \mu_i} + \frac{\partial}{\partial r}\frac{\partial E}{\partial \mu_i} - \frac{1}{r}\frac{\partial E}{\partial \mu_i}\right) J_1(\lambda r)\,dr\,. \tag{C2}$$

Integrate by parts to obtain

$$\left[\frac{\partial}{\partial r}\frac{\partial E}{\partial \mu_i} r J_1(\lambda r) - \frac{\partial}{\partial r}[rJ_1(\lambda r)]\frac{\partial E}{\partial \mu_i} - J_1(\lambda r)\frac{\partial E}{\partial \mu_i}\right]_0^\infty$$
$$+ \int_0^\infty \left\{r\frac{\partial^2}{\partial r^2}[rJ_1(\lambda r)] + \frac{\partial J_1(\lambda r)}{\partial r} - \frac{J_1(\lambda r)}{r}\right\}\frac{\partial E}{\partial \mu_i}\,dr\,. \tag{C3}$$

Since the Bessel function of first order equals zero at $r = 0$, and the electric field and its derivatives diminish at infinity, the boundary terms in the above equation are equal to zero. The integrand can be further simplified by expanding and reorganizing:

$$r\frac{\partial^2}{\partial r^2}[rJ_1(\lambda r)] + \frac{\partial J_1(\lambda r)}{\partial r} - \frac{J_1(\lambda r)}{r}$$
$$= r\frac{\partial^2}{\partial r^2}J_1(\lambda r) + 2\frac{\partial J_1(\lambda r)}{\partial r} - \frac{\partial J_1(\lambda r)}{\partial r} - \frac{J_1(\lambda r)}{r}$$
$$= r\left[\frac{\partial^2}{\partial r^2}J_1(\lambda r) + \frac{\partial J_1(\lambda r)}{r\partial r} - \frac{J_1(\lambda r)}{r^2}\right]. \tag{C4}$$

Let $\lambda r = R$, such that $(\partial/\partial r) = (\partial/\partial R)(\partial R/\partial r) = \lambda(\partial/\partial R)$. Carrying out this replacement in cooperation with the definition of the Bessel's function,

$$\left[\frac{\partial^2}{\partial R^2}J_1(R) + \frac{\partial J_1(R)}{R\partial R} - \frac{J_1(R)}{R^2}\right]R\lambda = -J_1(R)R\lambda\,, \tag{C5}$$

(C2) can be reduced to

$$\int_0^\infty -\frac{\partial E}{\partial \mu_i}J_1(\lambda r)\lambda^2\,dr = -\lambda^2\frac{\partial E(\lambda, z, \omega)}{\partial \mu_i}\,. \tag{C6}$$

The complete expression of the Henkel transformation for the partial derivative equation of $(\partial E/\partial \mu_i)$ is

$$\frac{\partial^2}{\partial z^2}\frac{\partial E}{\partial \mu_i} - u^2\frac{\partial E}{\partial \mu_i} = i\omega\psi_i(i\omega\varepsilon_0 + \sigma)E$$
$$+ \frac{1}{\mu_i}\frac{\partial E}{\partial z}[\delta(z - z_i) - \delta(z - z_{i+1})] + i\omega\frac{\partial \mu}{\partial z}\frac{\partial H_r}{\partial \mu_i}\,. \tag{C7}$$

APPENDIX D: EQUIVALENCE OF EQS (29) AND (32)

To prove that eq. (29) is equivalent to eq. (32), we only need to show that

$$\frac{G}{\mu_i}\frac{\partial E}{\partial z}\bigg|_{z_i}^{z_{i+1}} = \frac{2u_i^2\mu_0}{\mu_i}\left[\int_{z_i}^{z_{i+1}} G(\lambda, \omega, z)E(\lambda, \omega, z)\,dz - 2A_i b_i h_i\right]. \tag{D1}$$

For simplicity, we use G and E to denote $G(\lambda, \omega, z)$ and $E(\lambda, \omega, z)$. The generic solutions for the electric field and the Green's function in the ith layer take the following form:

$$\begin{aligned} E_i &= A_i \exp[u_i(z - z_i)] + B_i \exp[-u_i(z - z_i)]\,, \\ G_i &= a_i \exp[u_i(z - z_i)] + b_i \exp[-u_i(z - z_i)]\,. \end{aligned} \tag{D2}$$

Therefore,

$$2A_i b_i h_i = \int_{z_i}^{z_{i+1}} 2A_i b_i\,dz = \frac{1}{E_0}\int_{z_i}^{z_{i+1}} 2A_i B_i\,dz$$
$$= \frac{1}{2E_0}\int_{z_i}^{z_{i+1}}\left[E^2 - \frac{1}{u_i^2}\left(\frac{\partial E}{\partial z}\right)^2\right]dz$$
$$= \frac{1}{2}\int_{z_i}^{z_{i+1}}\left[EG - \frac{1}{u_i^2}\frac{\partial G}{\partial z}\frac{\partial E}{\partial z}\right]dz\,, \tag{D3}$$

where $E_0 = i\omega\mu_0 IaJ(\lambda a)\exp(u_0 z_{\mathrm{obs}})$. Inserting eq. (D3) back into the right-hand side of eq. (D1) results in

$$\frac{2u_i^2}{\mu_i}\left[\int_{z_i}^{z_{i+1}} G(\lambda, \omega, z)E(\lambda, \omega, z)\,dz - 2A_i B_i h_i\right]$$
$$= \frac{2u_i^2}{\mu_i}\int_{z_i}^{z_{i+1}}\left[\frac{GE}{2} + \frac{1}{2u_i^2}\frac{\partial G}{\partial z}\frac{\partial E}{\partial z}\right]dz$$
$$= \frac{1}{\mu_i}\int_{z_i}^{z_{i+1}}\left(u_i^2 GE + \frac{\partial G}{\partial z}\frac{\partial E}{\partial z}\right)dz$$
$$= \frac{1}{\mu_i}\int_{z_i}^{z_{i+1}}\left(G\frac{\partial^2 E}{\partial z^2} + \frac{\partial G}{\partial z}\frac{\partial E}{\partial z}\right)dz\,. \tag{D4}$$

Integrating by parts we obtain

$$\frac{1}{\mu_i}\int_{z_i}^{z_{i+1}}\left(G\frac{\partial^2 E}{\partial z^2} + \frac{\partial G}{\partial z}\frac{\partial E}{\partial z}\right)dz$$
$$= \frac{1}{\mu_i}\left\{G\frac{\partial E}{\partial z}\bigg|_{z_i}^{z_{i+1}} - \int_{z_i}^{z_{i+1}}\frac{\partial G}{\partial z}\frac{\partial E}{\partial z}dz + \int_{z_i}^{z_{i+1}}\frac{\partial G}{\partial z}\frac{\partial E}{\partial z}dz\right\}$$
$$= \frac{1}{\mu_i}G\frac{\partial E}{\partial z}\bigg|_{z_i}^{z_{i+1}}\,. \tag{D5}$$

APPENDIX E: COMPUTATION OF THE DISCRETE SENSITIVITIES

In the calculation of the sensitivities, we need to evaluate an integral f, defined by

$$f(\lambda, \omega, z) = \int_{z_i}^{z_{i+1}} G(\lambda, \omega, z) E(\lambda, \omega, z)\, dz = \frac{1}{E_0} \int_{z_i}^{z_{i+1}} E^2(\lambda, \omega, z)\, dz, \tag{E1}$$

with E_0 defined as in Appendix D. If we denote $E(\lambda, \omega, z)$ with E, then the partial differential equation for the electric field in the Hankel-transformed domain is

$$\frac{\partial^2 E}{\partial z^2} - u_i^2 = 0. \tag{E2}$$

Hence

$$f(\lambda, \omega, z) = \frac{1}{E_0} \int_{z_i}^{z_{i+1}} \frac{E}{u_i^2} \frac{\partial^2 E}{\partial z^2} dz = \frac{1}{E_0 u_i^2} \left\{ \left(E \frac{\partial E}{\partial z} \right) \Big|_{z_i}^{z_{i+1}} - \int_{z_i}^{z_{i+1}} \left(\frac{\partial E}{\partial z} \right)^2 dz \right\}. \tag{E3}$$

The general solution of eq. (E2) is a linear combination of up-going and down-going waves, as given in eq. (D2). Thus,

$$\int_{z_i}^{z_{i+1}} \left(\frac{\partial E}{\partial z} \right)^2 dz = \int_{z_i}^{z_{i+1}} E^2\, dz - 4 A_i B_i h_i. \tag{E4}$$

Inserting this equation back into eq. (E3) yields

$$f(\lambda, \omega, z) = \frac{1}{2 E_0 u_i^2} \left[E \frac{\partial E}{\partial z} \right]_{z_i}^{z_{i+1}} + 2 A_i B_i h_i. \tag{E5}$$

Since at the ith interface

$$\frac{\partial E_i}{\partial z} = \frac{\mu_i}{\mu_{i-1}} \frac{\partial E_{i-1}}{\partial z}, \tag{E6}$$

eq. (E1) can be, for the convenience of computation, further written as

$$f(\lambda, \omega, z) = \frac{1}{2 E_0 u_i^2} \left\{ \left[E_i \frac{\partial E_i}{\partial z} \right]_{z_{i+1}} - \frac{\mu_i}{\mu_{i-1}} \left[E_{i-1} \frac{\partial E_{i-1}}{\partial z} \right]_{z_i} \right\} + 2 A_i B_i h_i, \tag{E7}$$

where

$$\left[E_i \frac{\partial E_i}{\partial z} \right]_{z_{i+1}} = \frac{2 B_i Z^{i+1}}{Z^{i+1} + Z_i} \frac{B_i i \omega \mu_i}{Z^{i+1} + Z_i} \exp(-2 u_i h_i). \tag{E8}$$